η-nucleus interactions and in-medium properties of $N^*(1535)$ in chiral models

H. Nagahiro,[1] D. Jido,[2,*] and S. Hirenzaki[1]
[1]*Department of Physics, Nara Women's University, Nara 630-8506, Japan*
[2]*Research Center for Nuclear Physics, Osaka University, Ibaraki, Osaka 567-0047, Japan*
(Received 18 April 2003; published 17 September 2003)

The properties of η-nucleus interaction and their experimental consequences are investigated with η-nucleus optical potentials obtained by postulating the $N^*(1535)$ dominance for η-N system. The $N^*(1535)$ properties in the nuclear medium are evaluated by two kinds of chiral effective models based on distinct pictures of $N^*(1535)$. We find that these two models provide qualitatively different optical potentials of the η meson, reflecting the in-medium properties of $N^*(1535)$ in these models. In order to compare these models in physical observables, we calculate spectra of $(d,{}^3\mathrm{He})$ reactions for the η mesic nucleus formation with various kinds of target nuclei. We show that the $(d,{}^3\mathrm{He})$ spectra obtained in these models are significantly different and are expected to be distinguishable in experiments.

DOI: 10.1103/PhysRevC.68.035205 PACS number(s): 12.39.Fe, 14.20.Gk, 14.40.Aq, 25.10.+s

I. INTRODUCTION

The study of the in-medium hadron properties is one of the most interesting subjects in nuclear physics and has attracted continuous attention for decades. Historically, several kinds of hadron-nucleus bound systems were investigated such as pionic atoms, kaonic atoms, and $\bar{p}$ atoms [1]. Recently, the interests and importance of this field have been much increased due to both theoretical and experimental developments.

One of the important progresses in theoretical aspects is the new concept of partial restoration of chiral symmetry [2], in which a reduction of the order parameter of the chiral phase transition takes place in finite density and causes the modifications of the hadron properties. The development of the chiral effective theories enables us to discuss in-medium properties of hadrons in the viewpoint of chiral symmetry. In this context, hadronic bound systems have been investigated in various chiral models for pionic atoms [3,4], kaonic atoms/nuclei [5], and η and ω mesic nuclei [6–9].

Experimentally, the establishment of the $(d,{}^3\mathrm{He})$ spectroscopies in the formation of the deeply bound pionic atom opens new possibilities to form various kinds of hadron-nucleus bound systems, which are not accessible by the standard x-ray spectroscopies, and to investigate the bound states quite precisely. Originally the $(d,{}^3\mathrm{He})$ reaction was studied theoretically [10] as one of the proper methods to form the deeply bound pionic states [11], and later proved to be a powerful tool experimentally [12]. Using the $(d,{}^3\mathrm{He})$ reactions the deeply bound pionic $1s$ states were observed clearly and the binding energies and widths were determined precisely [3,12,13]. This method can be generalized to form other hadron-nucleus bound systems [6,14,15]. An experimental proposal to observe the η- and ω-nucleus system by the $(d,{}^3\mathrm{He})$ reactions at GSI has been approved already [16].

We investigate the η mesic nucleus in this paper. The special features of the η mesic nucleus are the following: (1) the η-N system dominantly couples to $N^*(1535)$ (N^*) at the threshold region [17]; (2) the isoscalar particle η filters out contamination of the isospin-3/2 excitation in the nuclear medium; and (3) as a result of the s-wave nature of the ηNN^* coupling, there is no threshold suppression like the p-wave coupling.

The dominant coupling of ηN to $N^*(1535)$ makes the use of this channel particularly suited to investigate this resonance and enables us to consider the η mesic nucleus as one of the doorways to investigate the in-medium properties of N^*. As shown in Ref. [6], the η-nucleus optical potential is extremely sensitive to the in-medium masses of N and N^* and even its qualitative nature may change from attractive to repulsive.

In this paper, we calculate the η-nucleus optical potential assuming the N^* dominance in η-N system, and use the chiral doublet models (the naive and mirror models) [18,19] and the chiral unitary model [8] to calculate the in-medium modification of N^*. These models are based on quite different pictures of N^*. In the chiral doublet model, the N and N^* form a multiplet of the chiral group. In Refs. [20,21], a reduction of the mass difference of the N and N^* in the nuclear medium is found in the chiral doublet model. On the other hand, an investigation of the η meson properties in the nuclear medium within a chiral unitary approach has been also reported [8]. There N^* is introduced as a resonance generated dynamically from meson-baryon scattering. Since this theoretical framework is quite different from the chiral doublet model, it is interesting to compare the consequences of these ''chiral'' models for N^* and η mesic nucleus.

For this purpose we calculate the $(d,{}^3\mathrm{He})$ spectra for various cases and show the numerical results. We find the significant differences for the spectra and can expect to distinguish the models from the experimental observables. Since the optical potential for η predicted with the chiral doublet model may change its nature from attractive to repulsive for higher nuclear densities, we even consider the η bound systems for unstable nuclei which are known to have low-

Present address: European Centre for Theoretical Studies in Nuclear Physics and Related Areas (ECT), Villa Tambosi, Strada delle Tabarelle 286, I-38050 Villazzano (Trento), Italy.

density halo structure in some nuclides. We would like to emphasize that we have possibilities to deduce the η-nucleus optical potential information from the experiments and obtain the N^* property in the medium which has a close connection to the N-N^* chiral dynamics.

In Sec. II, we describe the η-nucleus optical potentials obtained in the chiral doublet model by the naive and mirror assignments and in the chiral unitary model with assuming the N^* dominance in ηN channel. In Sec. III, we show the calculated $(d,{}^3\mathrm{He})$ spectra for the formation of the η-nucleus systems. Section IV is devoted to the summary.

II. CHIRAL MODELS FOR η-NUCLEUS INTERACTION

In this section, we show the formulation to calculate the η-optical potential in a nucleus. We use the chiral models that incorporate chiral symmetry in a different way in order to evaluate the in-medium behaviors of the N^* resonance.

In the recoilless $(d,{}^3\mathrm{He})$ reaction, which is proton picking-up process, the η meson can be created in the nucleus with small momentum. Therefore here we assume the η meson at rest in the nucleus.

A. General features of η-nucleus optical potential

First of all, we consider the η-nucleus optical potential within the N^* dominance hypothesis in the η-nucleon channel as discussed in Sec. I. If we assume the Lagrangian formulation for N^*, where N^* is described as a well-defined field and its propagator is written in the Breit-Wigner form, it is shown as a general conclusion that the η-nucleus optical potential is very sensitive to the in-medium difference of the N and N^* masses.

Considering an analogy to the isobar model for the Δ resonance in the π-N system, we obtain the η-optical potential in the nuclear medium in the heavy baryon limit [7] as

$$V_\eta(\omega)=\frac{g_\eta^2}{2\mu}\frac{\rho(r)}{\omega+m_N^*(\rho)-m_{N^*}^*(\rho)+i\Gamma_{N^*}(s;\rho)/2}, \quad (1)$$

where ω denotes the η energy and μ is the reduced mass of η and the nucleus. $\rho(r)$ is the density distribution for the nucleus. The ηNN^* vertex with the coupling constant g_η is given by

$$L_{\eta NN^*}(x)=g_\eta\overline{N}(x)\,\eta(x)N^*(x)+\mathrm{H.c.}, \quad (2)$$

where $g_\eta\simeq 2.0$ to reproduce the partial width $\Gamma_{N^*\to\eta N}\simeq 75$ MeV [17] at tree level. The ''effective masses'' $m_N^*(\rho)$ and $m_{N^*}^*(\rho)$ in the medium are defined as poles of their propagators so that $\mathrm{Re}\,G^{-1}(p^0=m^*,\vec{p}=0)=0$. Considering that the N^* mass in free space lies only 50 MeV above the ηN threshold and that in the medium the mass difference of N and N^* becomes smaller in the chiral doublet model, we expect that there is a critical density ρ_c where the sign of $\omega+m_N^*-m_{N^*}^*$ is getting to be positive. Then, the η-nucleus optical potential turns to be repulsive at density above ρ_c.

B. Chiral doublet model

In this section, we evaluate the effective masses of N and N^* using the chiral doublet model with the mirror and naive assignments in order to obtain the η-nucleus optical potential.

The chiral doublet model is an extension of the SU(2) linear σ model for the nucleon sector. There are two possible models in the chiral doublet model: the naive and mirror models [19,22]. In the latter model, N^* is regarded as the chiral partner of N and forms a chiral multiplet together with N. The Lagrangian density of the chiral doublet model with the mirror assignment is given by

$$\mathcal{L}=\sum_{j=1,2}\{\overline{N}_j i\partial\!\!\!/ N_j-g_j\overline{N}_j[\sigma+(-)^{j-1}i\gamma_5\vec{\tau}\cdot\vec{\pi}]N_j\}$$
$$-m_0(\overline{N}_1\gamma_5 N_2-\overline{N}_2\gamma_5 N_1), \quad (3)$$

where N_1 and N_2 are eigenvectors under the SU(2) chiral transformation. This Lagrangian was proposed and investigated first by DeTar and Kunihiro [18]. In the mirror assignment, N_1 and N_2 have an opposite axial charge to each other while they have the same charge in the ''naive'' assignment, which will be discussed later. The physical N and N^* are expressed as a superposition of N_1 and N_2 as $N=\cos\theta N_1+\gamma_5\sin\theta N_2$ and $N^*=-\gamma_5\sin\theta N_1+\cos\theta N_2$, where $\tan 2\theta=2m_0/\langle\sigma\rangle(g_1+g_2)$ [19], in order to diagonalize the mass terms after spontaneous breaking of chiral symmetry. The N and N^* masses are given by

$$m_{N,N^*}^*=\frac{1}{2}[\sqrt{(g_1+g_2)^2\langle\sigma\rangle^2+4m_0^2}\mp(g_2-g_1)\langle\sigma\rangle] \quad (4)$$

and the coupling constant of the πNN^* vertex also is given by

$$g_{\pi NN^*}=(g_2-g_1)/\sqrt{4+[(g_1+g_2)\langle\sigma\rangle/m_0]^2}, \quad (5)$$

where $\langle\sigma\rangle$ is the sigma condensate in the nuclear medium. The parameters in the Lagrangian have been chosen so that the observables in vacuum, $m_N=940$ MeV, $m_{N^*}=1535$ MeV, and $\Gamma_{N^*\to\pi N}\simeq 75$ MeV, are reproduced with $\langle\sigma\rangle_0=f_\pi=93$ MeV, and they are obtained as $g_1=9.8$, $g_2=16.2$, and $m_0=270$ MeV [19]. It is important here that the masses and couplings of N and N^* are constrained by chiral symmetry and are written as functions of the σ condensate. Such constraints are also observed in the chiral quartet model for $\Delta(1232)$ and $N(1520)$ with $J=3/2$ [23].

Assuming partial restoration of chiral symmetry in the nuclear medium, we parametrize the σ condensate as a function of the nuclear density ρ as

$$\langle\sigma\rangle=\Phi(\rho)\langle\sigma\rangle_0, \quad (6)$$

where, in the linear density approximation, $\Phi(\rho)=1-C\rho/\rho_0$ with $C=0.1$–0.3 [24]. The parameter C represents the strength of the chiral restoration at the nuclear saturation density ρ_0. In the mean field approximation, the medium

effects may be introduced by replacing the in-vacuum σ condensate by the in-medium one. Finally the in-medium mass difference is obtained by

$$m_N^*(\rho)-m_{N*}^*(\rho)=(1-C\rho/\rho_0)(m_N-m_{N*}). \tag{7}$$

As for the N^* width in the medium, we consider the two dominant decay channels of N^* in the medium, namely, $N^*\to\pi N$ and $NN^*\to\pi NN$ in this calculation. The other decay modes are shown to be negligible in our previous paper [6]. The $N^*\to\eta N$ channel does not contribute in the nuclear medium due to the Pauli blocking effects on the decayed nucleon and the $N^*\to\pi\pi N$ contribution is negligibly small in this model. The partial decay width for $N^*\to\pi N$ is calculated using the energy of N^* and is obtained as

$$\Gamma_\pi(s)=3\frac{g_{\pi NN*}^*}{4\pi}\frac{E_N+m_N^*}{\sqrt{s}}q, \tag{8}$$

where E_N and q are the energy and the momentum of the final nucleon on the mass shell in the rest frame of N^*, respectively. Similarly, we estimate the $NN^*\to\pi NN$ process within this model following the formulation of Ref. [7]:

$$\Gamma_{N*N\to\pi NN}(s) \tag{9}$$

$$=3\beta^2\left(\frac{g_{\pi NN}}{2m_N^*}\right)^2\rho\int dp_1p_1^3$$

$$\times\int\frac{dp_2}{(2\pi)^3p_2}\frac{m_N^*}{\omega_2}\frac{-\vec{p}_1^{\,2}+2m_N^*(\sqrt{s}-\omega_2-m_N^*)}{\left[\left(\frac{p_1^2}{2m_N^*}\right)^2-p_1^2-m_\pi^2\right]^2}$$

$$\times\Phi(p_1,p_2), \tag{10}$$

where p_1 (ω_1) and p_2 (ω_2) are pion momenta (energies) and Φ is the phase space variable defined in Ref. [7]. We define β as

$$\beta=\frac{g_1m_0}{\langle\sigma\rangle m_N^*(m_{N^*}^*+m_N^*)}\chi, \tag{11}$$

with the effective coupling of $\pi\pi NN^*$ through σ meson in this model, which is $\chi\sim1.29$. This contribution is estimated to be typically 15 MeV at the saturation density, although it depends on the η energy and the C parameter. We include this channel in the present calculation.

We also mention the naive assignment case in the chiral doublet model. The Lagrangian density for the naive assignment is given by

$$\mathcal{L}=\sum_{j=1,2}[\bar{N}_ji\partial\!\!\!/N_j+a_j\bar{N}_j(\sigma+i\gamma_5\vec{\tau}\cdot\vec{\pi})N_j]$$

$$+a_3\{\bar{N}_2(\gamma_5\sigma+i\vec{\tau}\cdot\vec{\pi})N_1-\bar{N}_1(\gamma_5\sigma+i\vec{\tau}\cdot\vec{\pi})N_2\}, \tag{12}$$

where $a_j(j=1,2,3)$ are the coupling constants. In the physical base, the masses of the N and N^* are given by

$$m_{N,N*}^*=\frac{\langle\sigma\rangle}{2}[\sqrt{(a_1+a_2)^2+4a_3^2}\mp(a_1-a_2)]. \tag{13}$$

The details of this model are discussed in Ref. [19]. As seen in Eq. (13), the mass difference of N and N^* is expressed as a linear function of $\langle\sigma\rangle$, which has exactly the same form as the mirror assignment case in Eq. (7). Therefore, as shown later, the general behavior of the η-optical potential obtained with the naive model is similar to that of the mirror model, since, essentially, the N-N^* mass difference is responsible for the qualitative change of the optical potential from attractive to repulsive in Eq. (1).

As for the N^* width in the medium, the two decay channels $N^*\to\pi N$ and $NN^*\to\pi NN$ are considered in the same manner as in the mirror assignment case. In the naive assignment, the σNN^* coupling vanishes under a diagonalization of the mass matrix. Hence, we consider additional terms given in Ref. [21], which describe quadratic meson-baryon interaction including the $\pi\pi NN^*$ coupling to calculate the width.

C. Chiral unitary model

We explain briefly another type of chiral model for baryon resonances, the chiral unitary approach [8,25], which is also used to describe the N^* resonance in the nuclear medium and to obtain the η-nucleus interaction. In this approach, a coupled channel Bethe-Salpeter equation for the meson-baryon scatterings is solved in vacuum, and N^* is generated dynamically as a resonance, contrary to the chiral doublet model, where the N^* field appears in the Lagrangian explicitly as explained in the preceding section.

To include the nuclear medium effects [8], they take into account the Pauli blocking of the intermediate nucleon states and use the in-medium propagators of the intermediate mesons (π,K,η) and baryons (N,Λ,Σ). The energy dependence of each self-energy is treated in a self-consistent manner. In this approach, the main component of the N^* is the $K\Sigma$ state [25], and the intermediate Σ is free from the Pauli blocking effect in the nuclear medium. Therefore, the medium modification of the N^* properties caused by the Pauli blocking effect on the intermediate nucleon is not large and, as a result of this fact, we think that they do not find significant changes of the mass and width of the N^* in the medium.

In the present paper, we directly take the η self-energy shown in Fig. 6(c) of Ref. [8(b)] calculated by the Valencia group as the results of the chiral unitary approach, and use it to obtain the η-nucleus optical potential.

III. NUMERICAL RESULTS

In this section, we show the numerical results on the η-nucleus optical potential and the formation cross sections of η-nucleus systems using the different models for η-nucleus interaction described in Sec. II.

A. η-nucleus interaction

The calculated η self-energy in the nuclear medium depends on the η energy and the nuclear density in general. We

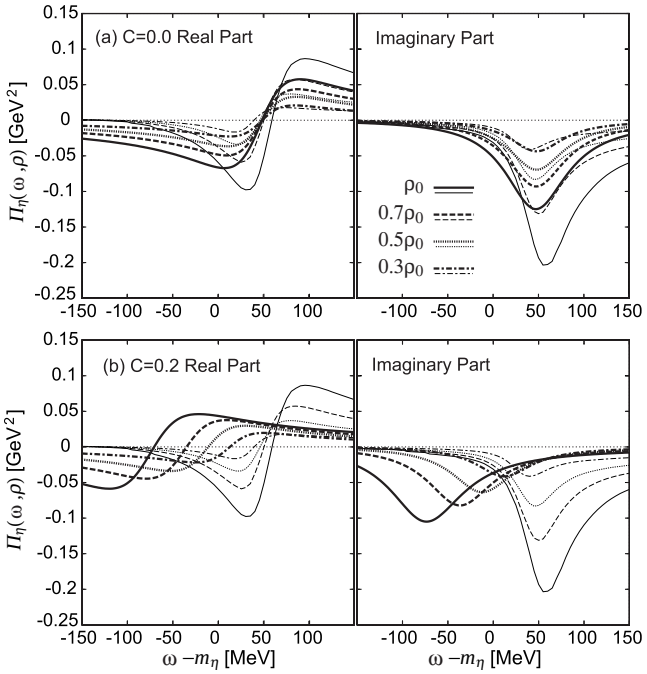

FIG. 1. The η self-energies are plotted as a function of the η energy for four nuclear density cases as indicated in the figure. (a) The self-energies obtained by the chiral doublet model with the mirror assignment for $C=0.0$ (thick lines) and those by the chiral unitary approach (thin lines). (b) Same as (a) except for $C=0.2$ for the chiral doublet model (thick lines). The results with the chiral unitary approach are taken from Fig. 6(c) of Ref. [8(b)] and are the same for both (a) and (b).

first show the calculated η self-energies in different models at finite nuclear density. In Fig. 1, we show the η self-energy at certain nuclear densities as a function of the energy carried by η. We compare the self-energies obtained by the chiral doublet model (the mirror assignment) with those obtained by the chiral unitary approach. We show the results for $C=0.0$ case in Fig. 1(a) and $C=0.2$ case in Fig. 1(b) for the chiral doublet model. The results with the chiral unitary approach are directly taken from Fig. 6(c) of Ref. [8(b)] and are the same in both Figs. 1(a) and 1(b). In the case of $C=0.0$ in the chiral doublet model, since there is no in-medium change of the sigma condensate $\langle\sigma\rangle$, the properties of N and N^* do not change in the medium. Therefore this case corresponds to the so-called "$t\rho$" approximation. We find that the self-energies of the chiral doublet model with $C=0.0$ resemble those of the chiral unitary approach. On the other hand, the results with $C=0.2$ show significant differences from the results of the chiral unitary approach, as can be seen in Fig. 1(b). Both real and imaginary parts of the self-energies of these two models show much different energy dependence for all nuclear densities considered here.

To see the consequences of these differences in the self-energy, we show in Fig. 2 the η-nucleus optical potential U defined as

$$U(r)=V(r)+iW(r)=\frac{1}{2m_\eta}\Pi_\eta(m_\eta,\rho(r)), \tag{14}$$

where the η energy is fixed to be m_η. The nuclear density is assumed to be of an empirical Woods-Saxon form here as

$$\rho(r)=\frac{\rho_0}{1+\exp\left(\dfrac{r-R}{a}\right)}, \tag{15}$$

where $R=1.18A^{1/3}-0.48$ fm and $a=0.5$ fm with the nuclear mass number A. We fix the η energy to its mass m_η here to see the r dependence of the optical potential. In all other numerical results shown in this paper, we use the appropriate energy dependent η-nucleus self-energies.

The optical potential is plotted in Fig. 2 for η-^{11}B system. We find that the potential with $C=0.0$ resembles that of the chiral unitary approach as expected from the behavior of the self-energies, and that it is essentially an attractive potential. However, the potential with $C=0.2$ has a repulsive core inside the nucleus as reported in Ref. [6] and is much different from the potential of the chiral unitary approach.

B. η-mesic nucleus formation by the $(d,{}^3\mathrm{He})$ reaction

In this section, we evaluate the formation rate of the η-nucleus system by the $(d,{}^3\mathrm{He})$ reaction and show the calculated results for various nuclear target cases. In the

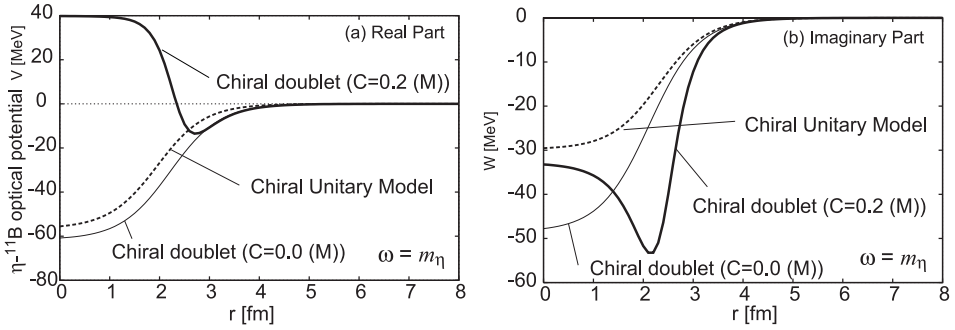

FIG. 2. The η-optical potentials for the η-^{11}B system as a function of the radius coordinate r. The left and right figures show the real part and the imaginary part, respectively. In both figures, the potentials of the chiral doublet model with the mirror assignment are shown in the solid lines for $C=0.2$ (thick line) and $C=0.0$ (thin line). The potential obtained using the chiral unitary model is shown by dotted line, which is obtained from the results shown in Ref. [8].

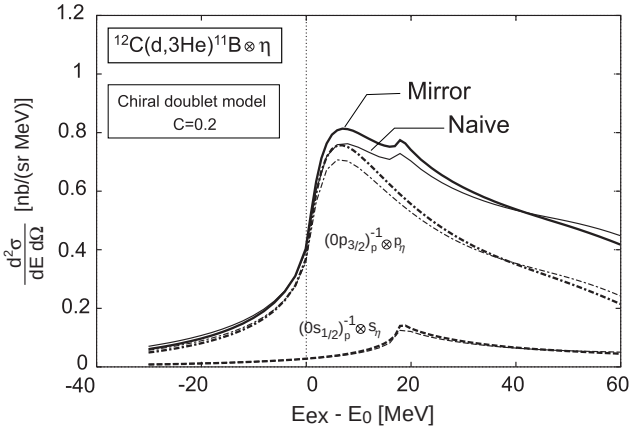

FIG. 3. The calculated spectra of ^{12}C$(d,^3$He) reaction at $T_d=3.5$ GeV for the formation of the η-^{11}B system are shown as functions of the excited energy $E_{\rm ex}$ defined in the text. E_0 is the η production threshold energy. Thick lines show the results with the mirror assignment and thin lines with the naive assignment. The dominant contributions from the $(0s_{1/2})_p^{-1}\otimes s_\eta$ and the $(0p_{3/2})_p^{-1}\otimes p_\eta$ configurations are shown by dashed lines and dash-dotted lines, respectively. Here, the proton-hole states are indicated as $(n\ell_j)_p^{-1}$ and the η states as ℓ_η.

$(d,^3$He) reaction spectroscopies, we only observe the emitted ^{3}He in the final state and obtain the double differential cross section $d\sigma/d\Omega/dE$ as a function of the ^{3}He energy. The energy of $\eta\otimes$nucleus system is evaluated from the ^{3}He kinetic energy and the properties of the η-nucleus interaction can be investigated from the $d\sigma/d\Omega/dE$ data. We use the Green function method to calculate the formation cross sections of quasistable η-nucleus system [26]. All the details of the application of the Green function method to the η system formation are found in Refs. [6,14]. In this paper, we consider $T_d=3.5$ GeV as the initial deuteron kinetic energy which satisfies the recoilless condition for the η production.

We show the ^{12}C $(d,^3$He) ^{11}B$\otimes\eta$ reaction cross sections for the formation of the η-^{11}B system in the final state in Fig. 3. The spectra obtained are shown as functions of the excited energy defined as

$$E_{\rm ex}=m_\eta-B_\eta+[S_p(j_p)-S_p(\text{ground})], \qquad (16)$$

where B_η is the η binding energy and $S_p(j_p)$ the proton separation energy from the proton single-particle level j_p. S_p(ground) indicates the separation energy from the proton level corresponding to the ground state of the daughter nucleus. The nuclear density distributions are assumed to be the empirical Woods-Saxon form defined in Eq. (15).

Here, we briefly explain the general features of the $(d,^3$He) spectra for the η production using Fig. 3. As shown in the figure, the spectrum is dominated by two contributions which are $(0s_{1/2})_p^{-1}\otimes s_\eta$ and $(0p_{3/2})_p^{-1}\otimes p_\eta$ configurations since the final states with the total spin $J\sim 0$ are largely enhanced in the recoilless kinematics. The η production threshold with the $(0p_{3/2})_p^{-1}$ proton-hole state is indicated by the vertical dotted line at $E_{\rm ex}-E_0=0$. The threshold with the $(0s_{1/2})_p^{-1}$ hole state, which is the excited state of the daughter nucleus, is at $E_{\rm ex}-E_0=18$ MeV because of the difference of $S_p(j_p)$ in Eq. (16). Thus, the contributions from the bound η states appear in the $E_{\rm ex}-E_0<0$ region with the $(0p_{3/2})_p^{-1}$ state and in the $E_{\rm ex}-E_0<18$ MeV region with the $(0s_{1/2})_p^{-1}$ state.

In the present case of Fig. 3, there are no bound states and the strength in the bound region is due to the absorptive interaction of η-nucleus system. The existence of the imaginary part in the potential, which accounts for η absorption in the nucleus, deforms the shape of the spectrum and provides certain strength in the subthreshold region. Hence, this subthreshold strength has no relation to the existence of the bound states. If we had the bound states with sufficiently narrow width, we would see the peak structure in the η bound region, which is not seen in Fig. 3.

In the higher excitation energy region, the calculated spectra show the contribution from the quasifree (positive energy) η production with a proton-hole state. Since the recoilless condition is satisfied only around $E_{\rm ex}-E_0\sim 0$, the cross section is smaller for the higher excitation energy due to the larger momentum transfer, even if the emitted quasifree η has the larger phase space.

Hence, the peak structure shown in Fig. 3 is the consequence of the reaction cross section around the η production threshold and does not have the direct connection to the existence of the bound states. However, the whole shape of the spectrum reflects the properties of the η-nucleus interaction and provides important information even if there are no quasistable bound peaks in the spectrum.

Going back to the discussion of our results, in Fig. 3, we show the calculated results by the chiral doublet model with both mirror and naive assignments. As expected in Sec. II B, both assignments predict similar $(d,^3$He) spectra and show the repulsive nature of the η-nucleus interaction. Hereafter, we only show the results with the mirror assignment since both assignments provide similar spectra.

In Fig. 4, we show the ^{12}C$(d,^3$He) ^{11}B$\otimes\eta$ spectra for three different η-nucleus optical potentials. In Fig. 4(a), the spectra with the so-called $t\rho$ optical potential, which are calculated by putting $C=0.0$ in the chiral doublet model, are shown. We show the spectra obtained by the chiral doublet model with $C=0.2$ in Fig. 4(b). We can see in the figures that the repulsive nature of the potential shifts the $(d,^3$He) spectrum to the higher energy region compared to the $t\rho$ case. In Fig. 4(c), we show the results by the chiral unitary model. As expected by the potential shape, the spectra with the chiral unitary approach are shifted significantly to the lower energy region as in the $t\rho$ potential case as a result of the attractive potential. We should mention here that we can see the contributions from the bound η states in Figs. 4(a) and 4(c) as bumps in dashed lines around $E_{\rm ex}-E_0=10$–15 MeV. We have found that there exist certain discrepancies between the spectra obtained with different chiral models, which are expected to be distinguished by the experimental data.

Next we consider the case of an unstable nuclear target. As shown in Fig. 2, since the chiral doublet model combines the possible existence of the attractive η-nucleus interaction

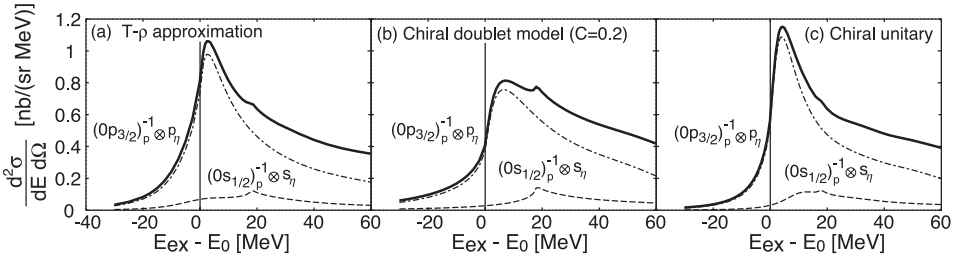

FIG. 4. The calculated spectra of ^{12}C$(d,^3$He$)^{11}$B$\otimes\eta$ reaction at $T_d=3.5$ GeV are shown as functions of the excited energy $E_{\rm ex}$ defined in the text. E_0 is the η production threshold energy. The η-nucleus interaction is calculated by (a) the $t\rho$ approximation, (b) the chiral doublet model with $C=0.2$, and (c) the chiral unitary approach. The total spectra are shown by the thick solid lines, and the dominant contributions from the $(0s_{1/2})_p^{-1}\otimes s_\eta$ and the $(0p_{3/2})_p^{-1}\otimes p_\eta$ configurations are shown by dashed lines and dash-dotted lines, respectively. Here, the proton-hole states are indicated as $(n\ell_j)_p^{-1}$ and the η states as ℓ_η.

at lower nuclear densities with the repulsive interaction at higher densities, it will be interesting to study the η mesic state in the unstable nuclei with halo structure [27]. Here, we consider ^{11}Li as an example of the halo nuclei and evaluate the cross section of the ^{12}Be$(d,^3$He$)$ reaction for the formation of the η-^{11}Li system in the final state.

The density distribution of ^{11}Li is determined from the experimental interaction cross sections [28] by using the cluster-orbital shell model approximation (COSMA) [29,30]. In this approximation, the nucleon density in ^{11}Li is expressed as the sum of the density in the ^{9}Li core and those of the two valence neutrons. For the ^{9}Li core, we use the Gaussian functional form for the proton and neutron densities, which reproduce the experimental rms radii as $R^p_{\rm rms}=R^n_{\rm rms}=R^{\rm exp}_{\rm mat}(^9{\rm Li})=2.32$ fm [28]. For the halo density, we consider two possibilities for the orbital angular momentum of the halo neutrons and apply the following two kinds of functional forms [29]:

$$\rho^{1s}(r)=\frac{1}{\pi^{2/3}\alpha_{1s}^3}\exp[-(r/\alpha_{1s})^2], \tag{17}$$

$$\rho^{1d}(r)=\frac{4r^4}{15\pi^{2/3}\alpha_{1d}^7}\exp[-(r/\alpha_{1d})^2], \tag{18}$$

where the range parameter α is determined to be $\alpha_{1s}=4.88$ fm and $\alpha_{1d}=3.2$ fm [29] so as to reproduce the experimental radius of ^{11}Li as $R^{\rm exp}_{\rm mat}(^{11}{\rm Li})=3.2$ fm [28].

For the density distribution of the target nucleus ^{12}Be, we sum up the square of the harmonic oscillator wave functions for all occupied states to obtain the point nucleon density. The oscillator parameter is determined by the experimental rms radius of ^{12}Be, $R_{\rm rms}(^{12}{\rm Be})=2.59$ fm [31]. To get the charge (matter) distribution of the ^{12}Be, we fold the point nucleon density with the Gaussian nucleon density with the size of $(R^N_{\rm rms})^2=0.69$ fm^2.

In Fig. 5, we show the calculated spectra for the formation of the $\eta\otimes^{11}$Li system by the ^{12}Be$(d,^3$He$)$ reaction. Here, we assume that the halo neutrons are in the $1s$ state and use Eq. (17) for the halo neutron density of the COSMA. We compare the results of the chiral doublet model with those of the chiral unitary model. In this case, we can see the repulsive nature of the chiral doublet prediction and the differences of the results of these models again. Both results have qualitatively the same features as the results shown in Fig. 4 for the ^{12}C target cases. However, the contributions from the $(0s_{1/2})_p^{-1}\otimes s_\eta$ configurations are relatively enhanced in the ^{12}Be target case because of the difference of the single-particle proton configuration in the target. In the total spectrum, we can clearly see the cusp due to the $(0s_{1/2})_p^{-1}\otimes s_\eta$ configurations, which could be interesting and useful to identify the η contributions in experiments.

To see the low-density halo contributions clearly, we show the results with halo neutrons in $1s$ state [Eq. (17)], in $1d$ state [Eq. (18)], and without halo neutron cases in Fig. 6 for the chiral doublet model and the chiral unitary model. In both models, we cannot see significant differences in the spectra due to the difference of the halo neutron states $1s$ or $1d$ in dominant contributions as shown in the figure. The

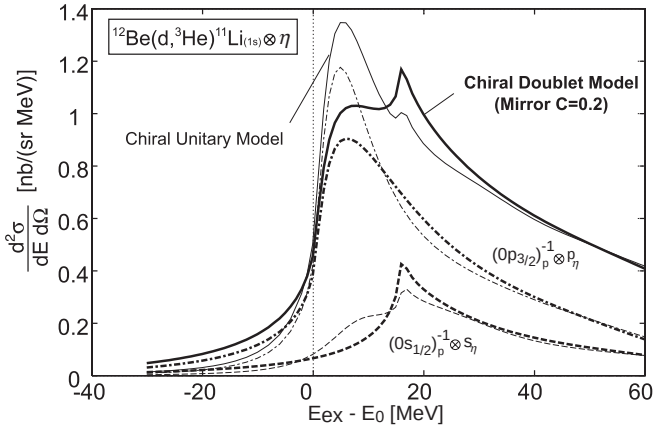

FIG. 5. The calculated spectra of ^{12}Be$(d,^3$He$)^{11}$Li$\otimes\eta$ reaction at $T_d=3.5$ GeV are shown as functions of the excited energy $E_{\rm ex}$ defined in the text. E_0 is the η production threshold energy. The η-nucleus interaction is calculated by the chiral doublet model with the mirror assignment with parameter $C=0.2$ (thick lines) and the chiral unitary model (thin lines). The total spectra are shown by the solid lines, and the contributions from the $(0s_{1/2})_p^{-1}\otimes s_\eta$ and the $(0p_{3/2})_p^{-1}\otimes p_\eta$ configurations are shown by dashed lines and dashed-dotted lines, respectively. Here, the proton-hole states are indicated as $(n\ell_j)_p^{-1}$ and the η states as ℓ_η. The ρ^{1s} form is used as the halo neutron density in the unstable ^{11}Li distribution (see text).

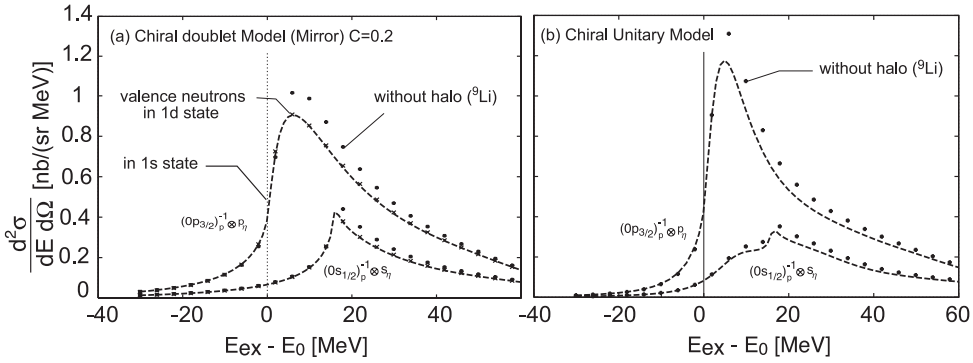

FIG. 6. The calculated spectra of ^{12}Be$(d,^3$He$)^{11}$Li$\otimes\eta$ reaction at $T_d=3.5$ GeV are shown as functions of the excited energy $E_{\rm ex}$ defined in the text. E_0 is the η production threshold energy. The η-nucleus interaction is calculated by (a) the chiral doublet model with the mirror assignment with the parameter $C=0.2$ and (b) the chiral unitary model. In each figure, the contributions from the $(0s_{1/2})_p^{-1}\otimes s_\eta$ and the $(0p_{3/2})_p^{-1}\otimes p_\eta$ configurations are shown. Here, the proton-hole states are indicated as $(n\ell_j)_p^{-1}$ and the η states as ℓ_η. The dashed lines indicate the results with the ρ^{1s} and the crosses with the ρ^{1d} halo neutron density distributions. The dots indicate the results from the ^{9}Li core calculated without halo neutron density.

spectra calculated without halo neutrons, which are thought to be equivalent to the contribution from the core ^{9}Li, have slightly larger cross sections in all the cases considered here. We think this enhancement is due to the lack of distortion effects in the final states from the halo neutrons.

From the results shown in Figs. 5 and 6, we think that it is difficult to observe the characteristic spectra due to the existence of the wide low-density region with the realistic halo neutron density distribution of ^{11}Li. In order to see the low-density-attractive nature of the optical potential predicted by the chiral doublet model, we need to consider the nuclei with more ''effective'' halo than ^{11}Li, which has larger spatial dimension and includes more neutrons, and may exist in the heavier mass region [32].

In all results shown above, we consider the target nuclei that include protons both in $s_{1/2}$ and $p_{3/2}$ states. In the $(d,^3$He) reactions with the recoilless condition, the substitutional configurations are known to be largely populated. Hence, to consider the target nucleus which includes only $s_{1/2}$ protons is interesting because the spectrum will be dominated by the only contribution $(0s_{1/2})_p^{-1}\otimes s_\eta$. We can expect to deduce the information of the η-nucleus interaction very easily without decomposing the spectrum into subcomponents. For this purpose, we consider ^{4}He as a target nucleus and calculate the $(d,^3$He) spectrum for the formation of the η-^{3}H system in the final state. Of course, we are aware of the lack of the few-body treatment in our formalism and we should improve it for a more quantitative calculation. However, we think it is still extremely interesting to evaluate the spectrum for the ^{4}He target case to see the advantages to observe the spectra with the single dominant subcomponent.

We show the calculated results of the ^{4}He$(d,^3$He$)^3$H $\otimes\eta$ reaction in Fig. 7. As we expected, the results are completely dominated by the single component and will be easily related to the behavior of the η-nucleus interaction and N^* properties in the medium. We can see the clear differences in the three cases here.

Finally, we show the results with the heavy target ^{40}Ca case in Fig. 8. In the heavier targets, we have larger possibilities to have bound states and larger medium effects. However, it seems to be very difficult to deduce the clear information from the spectra since many configurations $(n\ell_j)_p^{-1}\otimes\ell_\eta$ contribute to the spectra and they cannot be distinguished because of the large width. We calculate the ^{40}Ca$(d,^3$He$)^{39}$K$\otimes\eta$ spectrum with the chiral doublet model and see the experimental feasibilities to use the heavy target. We find that the whole spectrum is shifted according to the change of the C parameter in the model and we may be able to deduce the average strength of the potential from the position of the whole spectrum. However, as we expected, it seems extremely difficult and almost impossible to distinguish each contribution from the full spectrum.

IV. CONCLUSION

We have studied the properties of η-nucleus interaction and their experimental implications. We obtain the η-nucleus

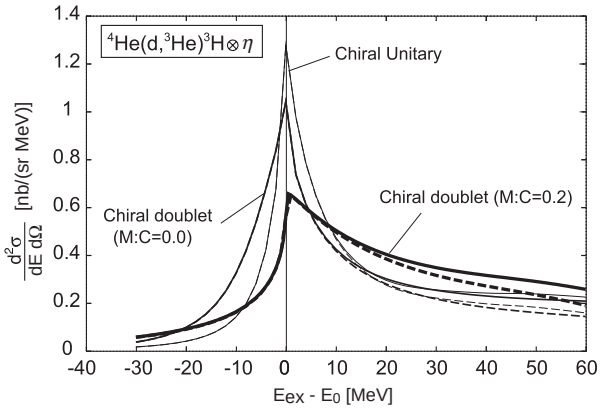

FIG. 7. The calculated spectra of ^{4}He$(d,^3$He$)^3$H$\otimes\eta$ reaction at $T_d=3.5$ GeV are shown as functions of the excited energy $E_{\rm ex}$ defined in the text. E_0 is the η production threshold energy. The η-nucleus interaction is calculated by the chiral doublet model with the mirror assignment with parameter $C=0.2$ (thick lines) and $C=0.0$ (medium lines) and the chiral unitary model (thin lines). In each figure, the contribution from the $(0s_{1/2})_p^{-1}\otimes s_\eta$ configuration is shown as the dashed line. Here, the proton-hole states are indicated as $(n\ell_j)_p^{-1}$ and the η states as ℓ_η.

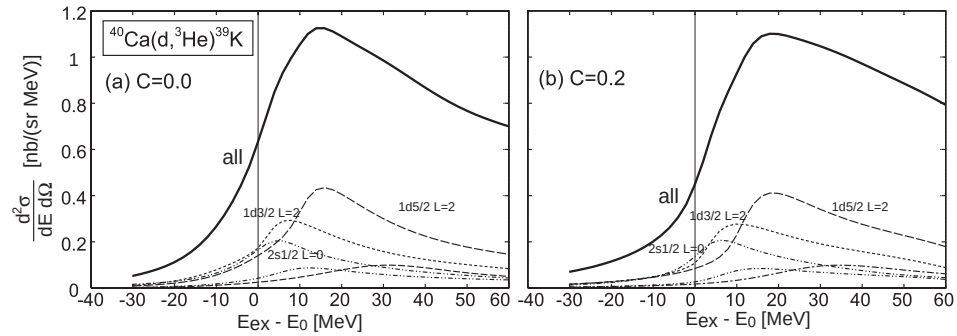

FIG. 8. The calculated spectra of ^{40}Ca(d,^{3}He) ^{39}K$\otimes\eta$ reaction at $T_d=3.5$ GeV are shown as functions of the excited energy $E_{\rm ex}$ defined in the text. E_0 is the η production threshold energy. The η-nucleus interaction is calculated by the chiral doublet model with the mirror assignment with parameter (a) $C=0.0$ and (b) $C=0.2$. In each figure, the full spectrum is shown by the thick solid line and dominant subcomponents are also shown as indicated in the figure.

optical potential by postulating the $N^*(1535)$ dominance in the η-N system. The $N^*(1535)$ properties in the nuclear medium are taken into account by two kinds of the chiral effective models: the chiral doublet model and the chiral unitary model.

We find that the two kinds of chiral models lead to the different properties of η-nucleus interaction as a result of the qualitatively different properties of N^* in the nuclear medium. Hence, the studies of the η-nucleus interaction can be connected to the properties of N^* in the medium and the information of the in-medium baryon chiral symmetries. Especially, we should stress here that the chiral doublet model leads to a unique shape of the η-nucleus optical potential which changes its nature from attractive to repulsive for higher nuclear densities. It could be extremely interesting to confirm the existence (or nonexistence) of this curious shape of the potential experimentally.

To investigate the experimental feasibility, we have calculated the (d,^{3}He) spectra for the formation of the η-nucleus systems in the final states. This (d,^{3}He) spectroscopy is an established experimental method in the studies of the pionic bound systems. We have studied theoretically the (d,^{3}He) spectra in a comprehensive manner and concluded that we can deduce the new information of η-nucleus interaction from the (d,^{3}He) experiment, and by knowing the nature of the η-nucleus optical potential, we will be able to study the in-medium properties of the N^*. We believe that this research helps much the experimental activities for the studies of the η-nucleus systems and the understanding of the baryon chiral symmetries and its medium modifications.

ACKNOWLEDGMENTS

This work was partly supported by Grants-in-Aid for Scientific Research (C) of the Japan Society for the Promotion of Science (JSPS), Grant No. 14540268.

[1] For example, see C.J. Batty, E. Friedman, and A. Gal, Phys. Rep. **287**, 385 (1997).
[2] See the reviews, T. Hatsuda and T. Kunihiro, Phys. Rep. **247**, 221 (1994); G.E. Brown and M. Rho, *ibid.* **269**, 333 (1996).
[3] P. Kienle, and T. Yamazaki, Phys. Lett. B **514**, 1 (2001); H. Geissel, *et al.*, *ibid.* **549**, 64 (2002); K. Suzuki *et al.*, nucl-ex/0211023.
[4] W. Weise, Acta Phys. Pol. B **31**, 2715 (2000); E.E. Kolomeitsev, N. Kaiser, and W. Weise, Phys. Rev. Lett. **90**, 092501 (2003).
[5] S. Hirenzaki, Y. Okumura, H. Toki, E. Oset, and A. Ramos, Phys. Rev. C **61**, 055205 (2000).
[6] D. Jido, H. Nagahiro, and S. Hirenzaki, Phys. Rev. C **66**, 045202 (2002); Nucl. Phys. **A721**, 665c (2003).
[7] H.C. Chiang, E. Oset, and L.C. Liu, Phys. Rev. C **44**, 738 (1991).
[8] (a) C. Garcia-Recio, J. Nieves, T. Inoue, and E. Oset, Phys. Lett. B **550**, 47 (2002); (b) T. Inoue and E. Oset, Nucl. Phys. **A710**, 354 (2002).
[9] F. Klingl, T. Waas, and W. Weise, Nucl. Phys. **A650**, 299 (1999).
[10] H. Toki, S. Hirenzaki, and T. Yamazaki, Nucl. Phys. **A530**, 679 (1991); S. Hirenzaki, H. Toki, and T. Yamazaki, Phys. Rev. C **44**, 2472 (1991).
[11] H. Toki and T. Yamazaki, Phys. Lett. B **213**, 129 (1988); H. Toki, S. Hirenzaki, T. Yamazaki, and R.S. Hayano, Nucl. Phys. **A501**, 653 (1989).
[12] H. Gilg *et al.*, Phys. Rev. C **62**, 025201 (2000); K. Itahashi, *et al.*, *ibid.* **62**, 025202 (2000).
[13] H. Geissel *et al.*, Phys. Rev. Lett. **88**, 122301 (2002).
[14] R.S. Hayano, S. Hirenzaki, and A. Gillitzer, Eur. Phys. J. A **6**, 99 (1999).
[15] K. Tsushima, D.H. Lu, A.W. Thomas, and K. Saito, Phys. Lett. B **443**, 26 (1998).
[16] R. S. Hayano *et al.*, GSI Report No. S214, 1997.
[17] Particle Data Group, K. Hagiwara *et al.*, Phys. Rev. D **66**, 010001 (2002).
[18] C. DeTar and T. Kunihiro, Phys. Rev. D **39**, 2805 (1989).
[19] D. Jido, M. Oka, and A. Hosaka, Prog. Theor. Phys. **106**, 873 (2001); D. Jido, Y. Nemoto, M. Oka, and A. Hosaka, Nucl. Phys. **A671**, 471 (2000).

[20] T. Hatsuda and M. Prakash, Phys. Lett. B **224**, 11 (1989).
[21] H. Kim, D. Jido, and M. Oka, Nucl. Phys. **A640**, 77 (1998).
[22] Y. Nemoto, D. Jido, M. Oka, and A. Hosaka, Phys. Rev. D **57**, 4124 (1998).
[23] D. Jido, T. Hatsuda, and T. Kunihiro, Phys. Rev. Lett. **84**, 3252 (2000).
[24] T. Hatsuda, T. Kunihiro, and H. Shimizu, Phys. Rev. Lett. **82**, 2840 (1999); D. Jido, T. Hatsuda, and T. Kunihiro, Phys. Rev. D **63**, 011901 (2000).
[25] N. Kaiser, P.B. Siegel, and W. Weise, Phys. Lett. B **362**, 23 (1995).
[26] O. Morimatsu and K. Yazaki, Nucl. Phys. **A435**, 727 (1985); **A483**, 493 (1988).
[27] For example, see I. Tanihata, J. Phys. G **22**, 157 (1996).
[28] I. Tanihata *et al.*, Phys. Rev. Lett. **55**, 2676 (1985).
[29] M.V. Zhukov *et al.*, Phys. Rep. **231**, 151 (1993).
[30] A.A. Korsheninnikov *et al.*, Phys. Rev. C **53**, R537 (1996).
[31] I. Tanitaha *et al.*, Phys. Lett. B **206**, 592 (1988).
[32] J. Meng and P. Ring, Phys. Rev. Lett. **80**, 460 (1998).